Available online at www.sciencedirect.com
ScienceDirect
Journal of Solid State Chemistry 181 (2008) 950–956
JOURNAL OF SOLID STATE CHEMISTRY
www.elsevier.com/locate/jssc

Size-tunable synthesis of tetrapod-like ZnS nanopods by seed-epitaxial metal-organic chemical vapor deposition

Tianyou Zhai[a,b], Yang Dong[a,b], Yaobing Wang[a,b], Zongwei Cao[a,b], Ying Ma[a,*], Hongbing Fu[a], Jiannian Yao[a,*]

[a]*Beijing National Laboratory for Molecular Sciences (BNLMS), Institute of Chemistry, Chinese Academy of Sciences, Beijing 100080, PR China*
[b]*Graduate School, Chinese Academy of Sciences, Beijing 100039, PR China*

Received 5 November 2007; received in revised form 13 January 2008; accepted 20 January 2008
Available online 5 February 2008

Abstract

Single-crystalline tetrapod-like ZnS nanopods were synthesized by a one-step seed-epitaxial metal-organic chemical vapor deposition (MOCVD) approach using cubic CdSe nanocrystals as the seeds. The diameters of the ZnS tetrapods can be easily tuned by changing the distances between the substrates and precursors. A possible growth mechanism is discussed on the basis of the heterostructure epitaxial growth. The ZnS tetrapod has a zinc CdSe nanocrystal core at the center with four wurtzite ZnS arms growing out from the core along four [0001] directions. Due to the lower temperature and versatility, this controllable seed-epitaxial method has potential as a general means of forming complex branching structures and may also offer opportunities for applications as building blocks for optoelectronic devices.

Keywords: ZnS; Seed-epitaxial; Semiconductors; Nanostructures; Chemical vapor deposition

1. Introduction

Semiconductor nanostructures have drawn much attention, because their novel properties make them potentially ideal functional components for nanometer-scale electronics and optoelectronics [1–3]. The design and preparation of nanomaterials with tunable physical and chemical properties is a tremendous challenge [4,5]. In the past decade, much effort has been made to control the size and shape of nanocrystals, since these parameters primarily determine their electronic and optical properties [6–9]. Even more applications and new functional materials might emerge if nanocrystals can be synthesized with complex shapes and well-defined three-dimensional (3D) architectures [10]. The tetrapod structures are of particular interest because of their promising potential for building blocks in solar cells, as active components in nanoscale transistors, as field emitters, and might open up new possibilities to create unique architectures that cannot be realized with spherical or rod-shaped nanocrystals [11–14]. Since the Alivisatos group first reported the synthesis of tetrapod-shaped CdSe nanocrystals using a complicated thermal decomposition of organometallic precursors [15], several techniques have been developed to prepare tetrapodal crystals. However, harsh conditions such as reactions in organic solvents or chemical vapor deposition at high temperatures are normally required.

To achieve controllable growth of the unusual tetrapod morphology, many efforts have been made to understand the growth mechanism, which continues to attract attention to the present day. In the case of the vapor-grown nanocrystals of II–VI semiconductors, many researchers have proposed the model of the tetrapod as formed by a saphalerite nucleus, onto which wurtzite arms have developed by continual growth from four equivalent {111} facets [16]. Hence, the large class of semiconductors exhibiting zinc blende–wurtzite polytypism [17] of semiconductors could be incorporated into the tetrapodal

*Corresponding authors. Fax: +86 10 82616517.
E-mail addresses: yingma@iccas.ac.cn (Y. Ma), jnyao@iccas.ac.cn (J. Yao).

0022-4596/$ - see front matter © 2008 Published by Elsevier Inc.
doi:10.1016/j.jssc.2008.01.032

structure by this concept. As we know, phase control and switching (nucleation in the zinc blende phase while growing in the wurtzite phase) are key steps in this process [18]. To control these steps, it is necessary to change the nucleation and growth environments to separate the nucleation and growth processes. Recently, limited phase control enabled the high-yield synthesis of tetrapod-shaped CdTe nanocrystals of a single material, which effectively arranged four quantum rods of the same composition around a central dot [19]; however, there are few reports on the heterostructure epitaxial growth in tetrapodal nanorods [20]. It is well known that the lattice mismatch between CdSe and ZnS is relatively small, and the epitaxial growth of the ZnS shell on the CdSe core has also been reported [21–23]. Besides, orientation-controlled ZnS nanowire bundles were grown on a thin CdSe film by Wang et al. [24]. The growth of these self-assembled nanoarchitectures is based on the crystallographic characteristics. This motivates us to design and fabricate ZnS tetrapods via epitaxial growth on cubic CdSe nanocrystals. The results give experimental evidence for the saphalerite nucleus model, and provide useful information in the study of tetrapod structures.

ZnS has been extensively investigated as an important wide-band-gap semiconductor (3.68 eV) [25,26]. It is one of the oldest and probably one of the most important materials in the electronics industry with a wide range of applications including light-emitting diodes, lasers, efficient phosphors in flat-panel displays, etc. [27–30]. As for 1D nanostructure, ZnS has been synthesized as nanowires, nanotubes, and nanobelts by several groups [31,32]. In this work, we fabricate the tetrapod-like ZnS nanopods by thermal decomposition of $Zn(S_2CNEt_2)_2$ powders at 420 °C using CdSe nanocrystals as the seeds. In this process, the sizes of the ZnS nanopods can be easily tuned by changing the distances between the substrates and precursors. In addition, because of the lower temperature and versatility, this new controllable seed-epitaxial method has potential as a general means of forming complex branching structures and may also offer opportunities for applications as building blocks for optoelectronic devices.

2. Experimental procedure

2.1. Materials

Analytical-grade reagents including cadmium acetate, methanol, chloroform, toluene, zinc bis(diethyldithiocarbamate) ($Zn(S_2CNEt_2)_2$), and high-purity selenium powder (99.9%) were purchased from Beijing Chemical Reagent Ltd. Co. of China. Trioctylphosphine (TOP, 90%, Alfa) and stearic acid (SA, 96%, Aldrich) were used as received without further purification.

2.2. Synthesis of CdSe nanocrystals

The CdSe nanocrystals were synthesized according to the method of literature [33,34]. Typically, the synthetic processes were carried out in an inert atmosphere and were performed using standard air-free techniques. A mixture of a specified amount of 0.46 g of $Cd(Ac)_2$ and 5.5 g of ligand SA in a 25 ml three-neck flask was heated to about 150 °C to obtain a colorless clear solution of Cd precursor; then the solution was cooled to room temperature and aged for 24 h, and this system was heated to 290 °C. At this temperature, 0.12 g of selenium in 2.0 ml of TOP solution was quickly injected, and then the system was reacted for 5 min at 270 °C. After reaction, the obtained colloid solutions were cooled and precipitated by methanol. The formed flocculent precipitate was centrifuged and the upper layer liquid was decanted, and then the isolated solid was dispersed in toluene. The above centrifugation and isolation procedure was repeated several times for purification of the nanocrystals. Finally, the purified nanocrystals were re-dispersed in toluene. The obtained cubic nanocrystals with particle size of about 4–5 nm were used as the seeds for the growth of tetrapod-like ZnS nanopods (Fig. S1).

2.3. Synthesis of tetrapod-like ZnS nanopods

The tetrapod-like ZnS nanopods were synthesized through a low-pressure thermal decomposition process

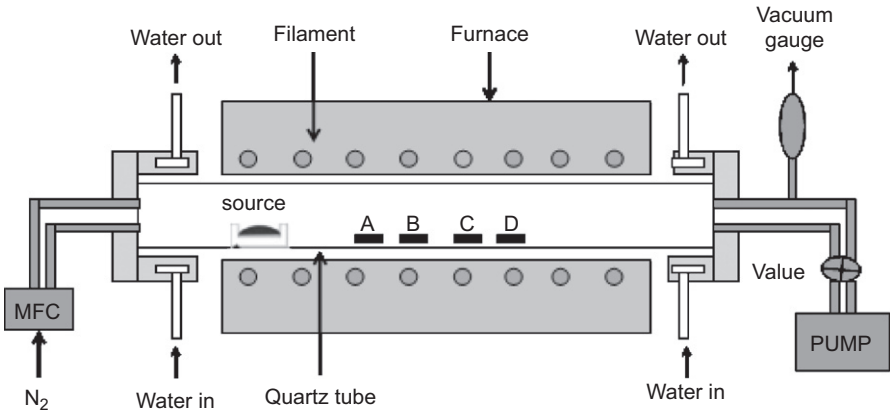

Fig. 1. Apparatus for the synthesis of tetrapodal ZnS nanorods.

described previously [35]. The apparatus is illustrated in Fig. 1. $Zn(S_2CNEt_2)_2$ powder was placed at the upstream end of the tube furnace and evacuated for several hours to purge oxygen in the chamber. After the elevation process was complete, the system was heated to 420 °C in 30 min and kept at this temperature for 120 min in a flowing atmosphere of N_2, which serves as both protecting medium and a carrying gas. During the heating process, the N_2 flow rate and pressure were kept at 60 sccm and 800 Pa, respectively. Single-crystal p-type Si substrates covered with cubic CdSe nanocrystals were placed on the high-temperature zone, and the distances between substrates and $Zn(S_2CNEt_2)_2$ powder were about 17, 19, 23, and 25 cm for samples A, B, C, and D, respectively. Thus, the ZnS tetrapods with different diameters could be obtained. The precursor was situated in advance according to the temperature gradient from the center to the ends of the furnace so that its temperature could be held at about 150 °C.

2.4. Measurement

The synthesized products were characterized by scanning electron microscopy (SEM, Hitachi F-4300) with X-ray energy dispersed spectrometry (EDS), X-ray diffraction (XRD, Rigaku D/max-2400PC) with Cu$K\alpha$ radiation, transmission electron microscope (TEM, JEOL JEM-1200EX), and high-resolution TEM (HRTEM, Philips Tecnai F30). X-ray photoelectron spectrum was measured using an ESCALab220i-XL electron spectrometer from VG Scientific using 300 W Al $K\alpha$ radiations. The binding energies were referenced to the C 1*s* line at 284.6 eV from adventitious carbon.

3. Results and discussion

The characteristic morphology of the tetrapod-like ZnS nanopods can be seen in the SEM images shown in Fig. 2. Overall, the products are uniform tetrapod-like nanocrystals, which are constituted of four nanopods with an average diameter of 80–100 nm and a length of 150–180 nm. Viewed more closely, as shown in Fig. 2d, the four arms of the nanocrystals conform to the same size and the surfaces of the nanopods are smooth. The angles between the arms are nearly the same, analogous to the spatial structure of molecular methane. Apart from the tetrapod-like nanocrystals, monopods, bipods, tripods, multipods (see circles in Fig. 2c), and pods congeries (Fig. 2a and b) are also obtained. The diameters of the nanopods and the arms of tetrapod-like nanocrystals are uniform on the whole. Similar to the typical chemical vapor deposition technique, the morphology of the ZnS tetrapods is sensitive to several experimental conditions, such as reaction temperature, deposition time, and carrier gas rate, possibly due to their preferential growth, as explained later. In this work, we found that the sizes of the nanopods can be easily tuned by changing the distances between the substrates and precursors, while the temperatures are almost the same. With increasing the distances, the as-grown ZnS nanopods with different mean diameters were sorted out into different groups: 250 nm (sample A),

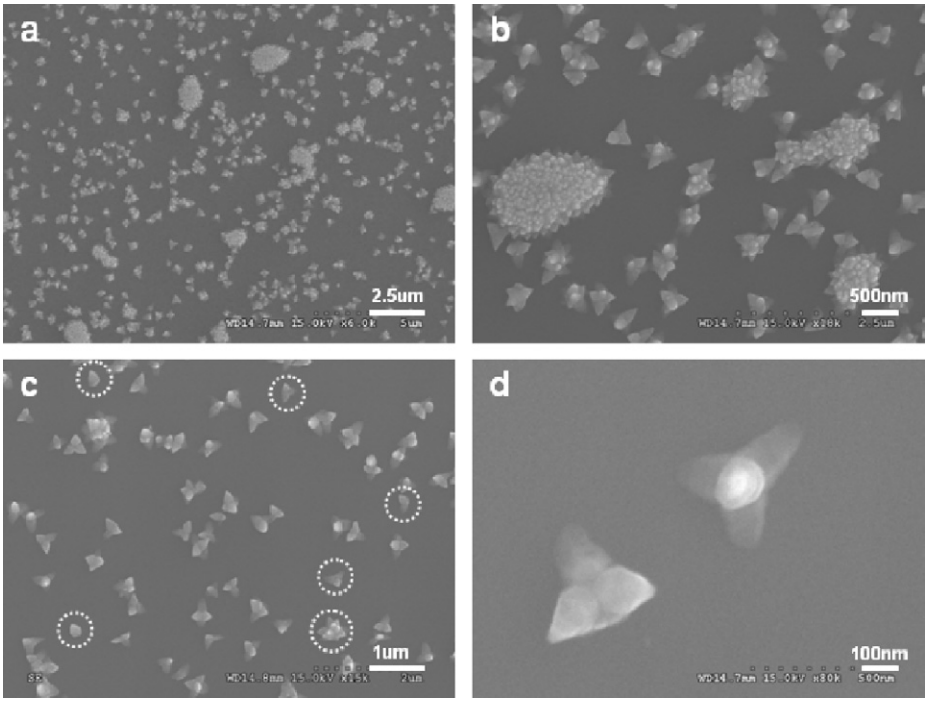

Fig. 2. SEM images of tetrapod-like ZnS nanopods (sample C).

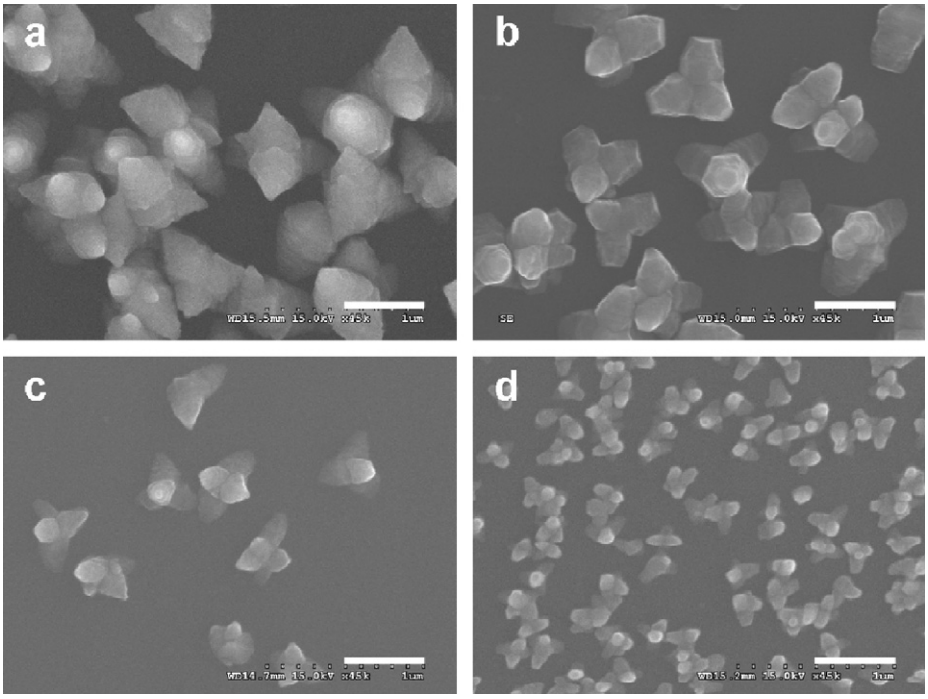

Fig. 3. SEM images of samples A–D, all scale bars are 500 nm.

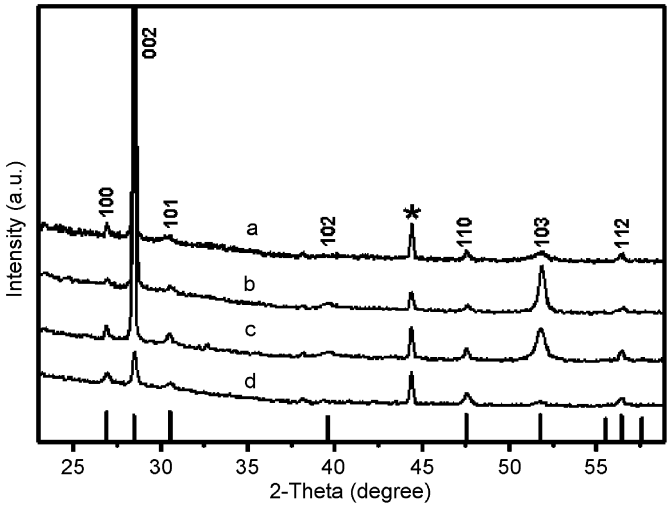

Fig. 4. XRD patterns of samples A–D.

180 nm (sample B), 100 nm (sample C), and 70 nm (sample D), as shown in Fig. 3.

The XRD patterns of samples A–D are shown in Fig. 4. All the diffraction peaks can be readily indexed as hexagonal wurtzite-structured ZnS, with the lattice constants $a = 3.785$ Å and $c = 6.186$ Å, which match well those listed in the JCPDS card no. 36-1450. No peaks belonging to cubic CdSe nanocrystals are observed in the XRD pattern due to the small size or low amount. The sharp diffraction peaks indicate the good crystallinity of the prepared crystals. Moreover, it is noted that the relative intensities of the peaks differ from the standard pattern of the bulk material, which should be caused by preferred orientation and distribution of ZnS nanopods. Patterns of all samples show a strong {002} diffraction peak, which might be due to the growth of wurtzite-structured ZnS along the [0001] direction.

X-ray photoelectron spectroscopy (XPS) was also measured to derive composition information of the product. Fig. 5 shows the XPS spectra obtained from the Zn and S regions of representative sample D. The binding energies obtained in the XPS analysis were corrected for specimen charging by reference to C 1*s* at 284.60 eV. The Zn $2p_{3/2}$ and S $2p_{3/2}$ features shown in Fig. 4a and b have binding energy $E_B = 1021.3$ and 161.4 eV, respectively. These results are in agreement with those of Refs. [36,37]. Quantification of these peaks reveals that the atomic ratio of Zn to S is about 1:1. Those data of the other samples are similar to that of sample D. Both XRD and XPS analyses indicate that the as-prepared products are ZnS.

Careful TEM examinations using low- and high-magnification imaging shed additional light on the structure of these tetrapod-like ZnS nanopods. Fig. 6a displays a low-magnification image in which the ZnS nanopods are quite uniformly distributed upon a copper grid. In Fig. 6b, one branch is nearly overlapped, which leads to the structure appearing as if it had only three branches. The diameters of the branches are about 70 nm, in agreement with the SEM results shown in Fig. 3d. Energy-dispersive X-ray spectra (EDS) of the tetrapod branch and core parts were analyzed to check their composition. From the EDS analyses, only zinc and sulfide were found in the projected branch region; in the projected core region, cadmium and selenium were

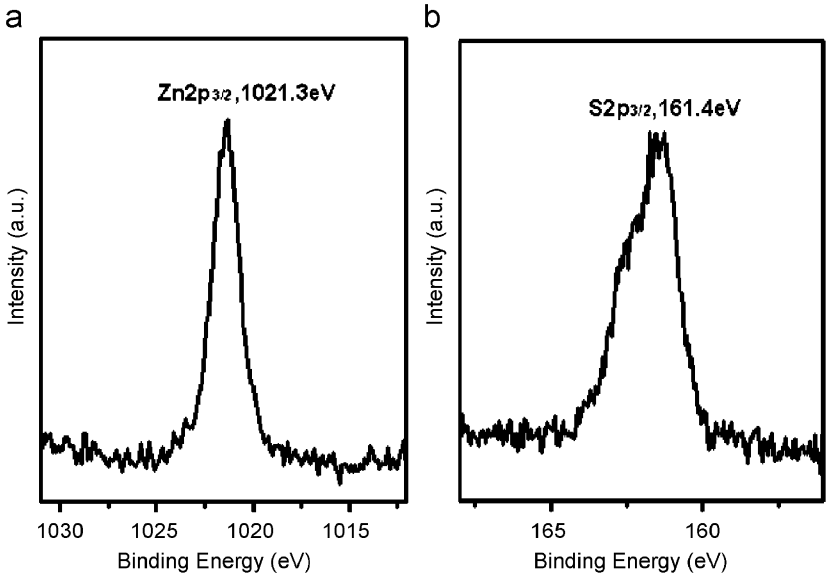

Fig. 5. XPS analysis of tetrapod-like ZnS nanopods (sample D): (a) zinc region; (b) sulfide region.

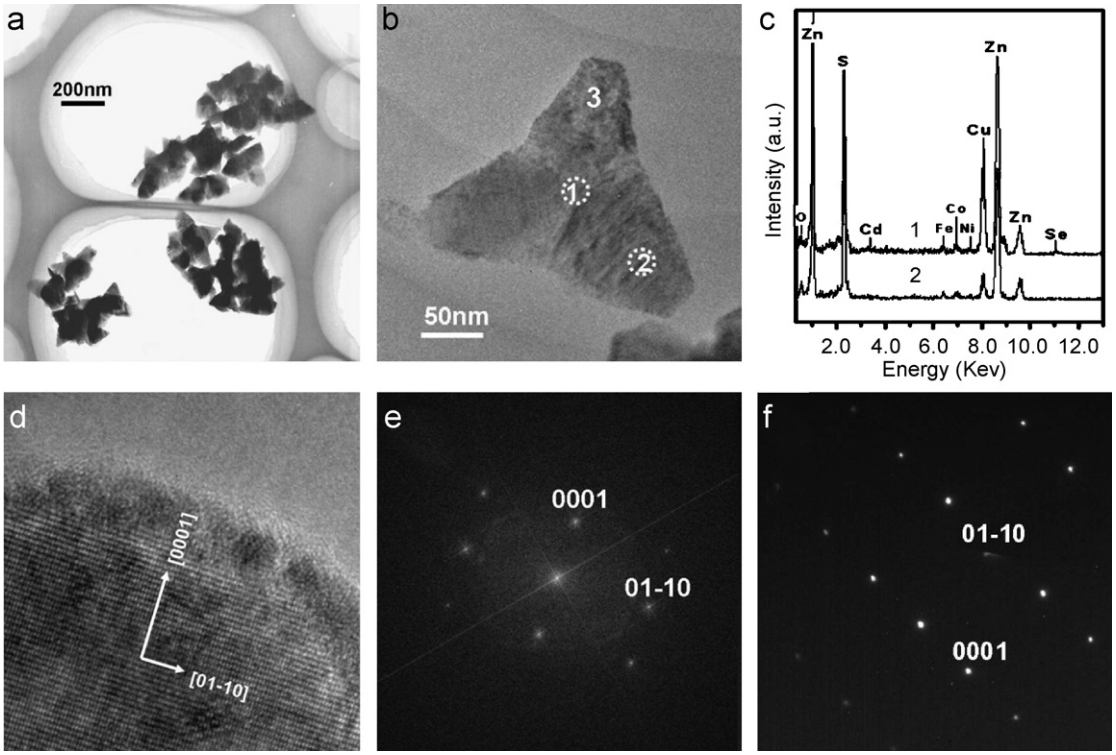

Fig. 6. TEM and HRTEM images of the tetrapod-like ZnS nanopods (sample D). (a) TEM image showing many ZnS nanopods; (b) an image of a single tetrapod; (c) energy-dispersive X-ray spectra on regions 1 and 2 in (b), in which the Fe, Co, Ni, Cu, and C peaks were generated from the supporting carbon-coated copper meshes; (d, e) HRTEM image and corresponding FFT image on region 3; (f) electron diffraction pattern taken from region 2.

also detected, which confirmed that the CdSe nanocrystal was in the core of the tetrapod-like structure. In these spectra, the other signals arise from the TEM grid or the pole piece of the TEM instrument. Detailed structure analysis of the as-synthesized ZnS nanopod was performed with HRTEM and electron diffraction (ED). Fig. 6d is an HRTEM image of a single branch within the architecture. The lattice fringes of the {010} and {001} planes are clearly seen with d spacing of ~0.33 and ~0.62 nm, respectively, which are characteristic of the wurtzite ZnS crystal structure. The corresponding fast Fourier transform (FFT) image shows a six-fold symmetric pattern that is readily indexed to the [100] zone axis of a wurtzite ZnS. Extensive HRTEM and ED examinations verify that all

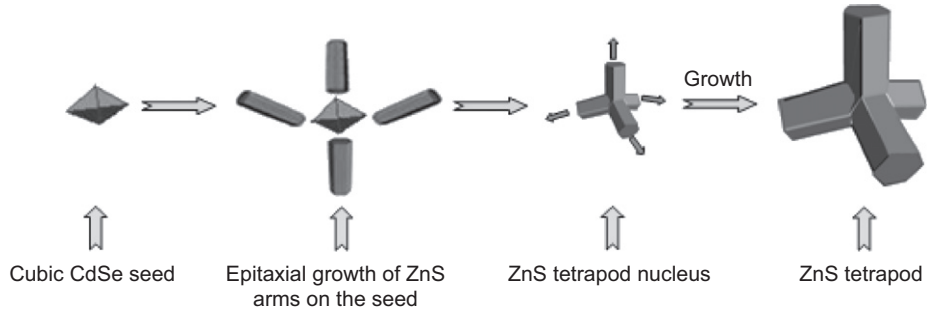

Fig. 7. Proposed growth mechanism of the tetrapod-like ZnS nanopods; see text for details.

branches of each tetrapod are structurally uniform and are, in fact, single crystals that grow along the [0001] direction. All attempts to obtain suitable lattices of cubic CdSe core have proven unsuccessful because the CdSe core was buried too deeply in the complex structure to obtain HRTEM images.

On the basis of the above analysis, the formation process of the tetrapod-like ZnS nanopods can be proposed, a schematic description of which is given in Fig. 7. It is worth mentioning that no branched nanostructure growth was observed on the same substrate in the absence of the CdSe nanocrystals. At the beginning, the $Zn(S_2CNEt_2)_2$ vapor generated by thermal evaporation is transported by the carrier gas to the substrates located at the high-temperature zone, and then decomposed to form ZnS vapor. Owing to the need for excess energy for nucleation, the newly arrived ZnS vapor prefers depositing on the CdSe seeds, and epitaxial growth of wurtzite-structured arms occurs on the seeds. When four wurtzite arms grow equivalently out of the four {111} equivalent faces of a tetrahedral zinc blende seeds, a tetrapod-shaped ZnS nucleus is obtained. This behavior is well known, and is due to the small energy difference between stacking sequences in the growth direction. However, the growth behavior on the substrate surface owing to the spatial hindrance was quite different from that in a homogeneous liquid phase, where the core nanocrystals were subjected to the same microenvironment. Furthermore, a fluctuation in vapor distribution could alter the microenvironment of the cubic CdSe nanocrystals. The equilibrium between growth on the four {111} faces is thus expected to break, which induces nanosynchronous growth of wurtzite arms from either one, two, or three {111} faces of a tetrahedral seed, resulting in the formation of monopod, bipod, and tripod nuclei. On the other hand, due to the fact that nanocrystals were not dispersed uniformly on the substrate, there are some regions where the CdSe nanocrystals were assembled together, which causes multipod-nuclei formation. Furthermore, these pod-like nuclei would continue growing easily with further deposition of ZnS vapor. From zones A to D, the distance between the substrates and precursors increases, and the degree of supersaturation and diffusion rate of ZnS molecules decrease, resulting in the formation of smaller tetrapods.

4. Conclusions

In conclusion, tetrapod-like ZnS nanopods were synthesized by a one-step seed-epitaxial MOCVD approach using CdSe nanocrystals as the seeds. In this process, the diameters of the tetrapod-like ZnS nanopods can be easily tuned by changing the distances between the substrates and precursors. These nanopods are single crystalline wurtzite ZnS branches with the cubic CdSe cores. This specific structure of CdSe-cored tetrapod-like ZnS nanopods may have potential application in nanoelectronics and photonics. Although the detailed growth mechanism requires more systematic investigations, the present results suggest that this simple method might be useful for the synthesis of many other complex semiconductor nanostructures to meet the growing demands of nanoscale science and technology.

Acknowledgments

This work was supported by the National Natural Science Foundation of China (Nos. 50221201, 90301010), the Chinese Academy of Sciences, the National Research Fund for Fundamental Key Projects No. 973 (2006CB806200). We thank Prof. Yongfang Li and Dr. Haizheng Zhong, Institute of Chemistry, Chinese Academy of Sciences, for their helpful discussions.

Appendix A. Supplementary materials

Supplementary data associated with this article can be found in the online version at doi:10.1016/j.jssc.2008.01.032.

References

[1] X.F. Duan, Y. Huang, R. Argarawal, C.M. Lieber, Nature 421 (2003) 241–245.
[2] Y.Y. Wu, H.Q. Yan, M. Huang, B. Messer, J.H. Song, P.D. Ang, Chem. Eur. J. 8 (2002) 1261–1268.
[3] M.S. Gudiksen, L.J. Lauhon, J. Wang, D. Smith, C.M. Lieber, Nature 415 (2002) 617–620.
[4] X.H. Zhong, R.G. Xie, L.T. Sun, I. Lieberwirth, W. Knoll, J. Phys. Chem. B 110 (2006) 2–4.
[5] C.M. Lieber, Z.L. Wang, MRS Bull. 32 (2007) 99–108.

[6] A.P. Alivisatos, Science 271 (1996) 933–937.
[7] H.Q. Yan, R.R. He, J. Pham, P.D. Yang, Adv. Mater. 15 (2003) 402–405.
[8] H.Z. Zhong, Y.C. Li, Y. Zhou, C.H. Yang, Y.F. Li, Nanotechnology 17 (2006) 772–777.
[9] T.Y. Zhai, H.Z. Zhong, Z.J. Gu, A.D. Peng, H.B. Fu, Y. Ma, Y.F. Li, J.N. Yao, J. Phys. Chem. C 111 (2007) 2980–2986.
[10] J.Q. Hu, Y. Bando, D. Golberg, Small 1 (2005) 95–99.
[11] Q. Pang, L.J. Zhao, Y. Cai, D.P. Nguyen, N. Regnault, N. Wang, S.H. Yang, W.K. Ge, R. Ferreira, G. Bastard, J.N. Wang, Chem. Mater. 17 (2005) 5263–5267.
[12] Y.C. Zhu, Y. Bando, D.F. Xue, D. Golberg, J. Am. Chem. Soc. 125 (2003) 16196–16197.
[13] B.Q. Sun, E. Marx, N.C. Greenham, Nano Lett. 3 (2003) 961–963.
[14] Y.F. Qiu, S.H. Yang, Adv. Funct. Mater. 17 (2007) 1345–1352.
[15] L. Manna, E.C. Scher, A.P. Alivisatos, J. Am. Chem. Soc. 122 (2000) 12700–12706.
[16] L. Carbone, S. Kudera, E. Carlino, W.J. Parak, C. Giannini, R. Cingolani, L. Manna, J. Am. Chem. Soc. 128 (2006) 748–755.
[17] C.Y. Yeh, Z.W. Lu, S. Proyen, A. Zunger, Phys. Rev. B 46 (1992) 10086–10097.
[18] Y.C. Li, H.Z. Zhong, R. Li, Y. Zhou, C.H. Yang, Y.F. Li, Adv. Funct. Mater. 16 (2006) 1705–1716.
[19] L. Manna, D.J. Milliron, A. Meisel, W.C. Scher, A.P. Alivisatos, Nature 2 (2003) 382–385.
[20] D.J. Milliron, S.M. Hughes, Y. Cui, L. Manna, J.B. Li, L.W. Wang, A.P. Alivisatos, Nature 430 (2004) 190–195.
[21] B.O. Dabbousi, J. Rodriguez-Viejo, F.V. Mikulec, J.R. Heine, H. Mattoussi, R. Ober, K.F. Jensen, M.G. Bawendi, J. Phys. Chem. B 101 (1997) 9463–9475.
[22] D.V. Talapin, I. Mekis, S. Götzinger, A. Kornowski, O. Benson, H. Weller, J. Phys. Chem. B 108 (2004) 18826–18831.
[23] L. Manna, E.C. Scher, L.S. Li, A.P. Alivisatos, J. Am. Chem. Soc. 124 (2002) 7136–7145.
[24] D.F. Moore, Y. Ding, Z.L. Wang, J. Am. Chem. Soc. 126 (2004) 14372–14373.
[25] X.H. Zhang, Y. Zhang, Y.P. Song, Z. Wang, D.P. Yu, Physica E 28 (2005) 1–6.
[26] D. Moore, Z.L. Wang, J. Mater. Chem. 16 (2006) 3898–3905.
[27] Z.W. Wang, L.L. Daemen, Y.S. Zhao, C.S. Zha, R.T. Downs, X.D. Wang, Z.L. Wang, R.J. Hemley, Nat. Mater. 4 (2005) 922–927.
[28] J.F. Gong, S.G. Yang, H.B. Huang, J.H. Duan, H.W. Liu, X.N. Zhao, R. Zhang, Y.W. Du, Small 2 (2006) 732–735.
[29] Y. Jiang, X.M. Meng, J. Liu, Z.R. Hong, C.S. Lee, S.T. Lee, Adv. Mater. 15 (2003) 1195–1198.
[30] Z.X. Zhang, J.X. Wang, H.J. Yuan, Y. Gao, D.F. Liu, L. Song, Y.J. Xiang, X.W. Zhao, L.F. Liu, S.D. Luo, X.Y. Dou, S.C. Mou, W.Y. Zhao, S.S. Xie, J. Phys. Chem. B 109 (2005) 18352–18355.
[31] D. Moore, Y. Ding, Z.L. Wang, Angew. Chem. Int. Ed. 45 (2006) 5150–5154.
[32] Y.F. Hao, G.W. Meng, Z.L. Wang, C.H. Ye, L.D. Zhang, Nano Lett. 6 (2006) 1650–1655.
[33] Z.A. Peng, X.G. Peng, J. Am. Chem. Soc. 124 (2002) 3343–3353.
[34] C.B. Murray, D.J. Norris, M.G. Bawendi, J. Am. Chem. Soc. 115 (1993) 8706–8715.
[35] C.J. Barrelet, Y. Wu, D.C. Bell, C.M. Lieber, J. Am. Chem. Soc. 125 (2003) 11498–11499.
[36] G.T. Zhou, X.C. Wang, J.C. Yu, Cryst. Growth Des. 5 (2005) 1761–1765.
[37] T.Y. Zhai, Z.J. Gu, H.B. Fu, Y. Ma, J.N. Yao, Cryst. Growth Des. 7 (2007) 1388–1392.